Modeling the three-dimensional upper ocean heat budget and subduction rate during the Subduction Experiment

Michael A. Spall, Robert A. Weller, and Peter W. Furey

Department of Physical Oceanography, Woods Hole Oceanographic Institution, Woods Hole, Massachusetts

Abstract. A global three-dimensional primitive equation general circulation model is used to estimate the upper ocean heat budget and subduction rates in the eastern North Atlantic during the period of the Subduction Experiment, June 1991 through July 1993. The seasonal cycle is dominated by one-dimensional processes throughout the subtropical gyre, i.e., a local balance between the net heat flux into the ocean through the surface and a vertical redistribution due to vertical mixing. However, closure of the heat budget on long timescales involves redistribution by Ekman transports (both horizontal and vertical), geostrophic advection, and vertical diffusion. Subgridscale parameterizations of eddy processes weakly restratify the upper ocean. The annual rate at which waters are subducted from the mixed layer into the permanent thermocline is estimated using both kinematic and thermodynamic methods. These subduction rates and patterns are generally consistent with each other and also with previous estimates of the large-scale subduction rate based on climatologies and models. Consideration of a finite thickness Ekman layer is shown to reduce the thermodynamic estimate of the subduction rate at low latitudes by $O(50\%)$, in much better agreement with the kinematic method. The effects of convergent eddy fluxes in the mixed layer and a diabatic thermocline on the subduction rate are also calculated and found to be small but not negligible. The seasonal and interannual evolution of the sea surface temperature and mixed layer depth in the model compare well with in situ measurements at five mooring locations taken as part of the Subduction Experiment. These results demonstrate that a global, low-resolution general circulation model forced with surface fluxes of heat and freshwater can accurately reproduce the evolution of the upper ocean thermal structure and provide a useful tool for the analysis of air-sea interaction and climate variability on seasonal to interannual timescales.

1. Introduction

Subduction is the process by which the near-surface waters within the region of strong turbulent mixing forced by the atmosphere are transferred into the more strongly stratified, less turbulent ocean interior. The correspondence between the water mass properties found at the surface in winter and the properties on these same isopycnal surfaces within the permanent thermocline in the subtropical gyres was first noted by *Montgomery* [1938] and *Iselin* [1939]. *Stommel* [1979] proposed that the large seasonal cycle in mixed layer depth would selectively choose the late winter properties (i.e., active tracers such as temperature, salinity, potential vorticity, and passive chemical tracers) to be subducted into the stratified interior where, because of weak mixing, the properties would remain nearly constant. Thus the process by which water is subducted from the near surface, where it is in contact with the atmosphere, into the ocean interior is central to the determination of the large-scale oceanic circulation, stratification, water mass properties, and oceanic uptake of chemicals from the atmosphere.

In an effort to understand better the subduction process the Subduction Experiment was carried out in the eastern subtropical North Atlantic between June 1991 and July 1993. This region was chosen because of the typically large-scale patterns that dominate the surface forcing, including the anticyclonic

curl of the wind stress associated with the Azores/Bermuda High, because of the relatively low eddy kinetic energy levels and because prior work had suggested that subduction was taking place there [*Montgomery*, 1938; *Stommel*, 1979; *Jenkins*, 1987].

The present study focuses on large-scale processes that contribute toward the subduction. The convergence of the surface flow forced by the large-scale wind stress pattern pumps water downward at the base of the mixed layer. Horizontal advection may carry water parcels from the mixed layer into the stratified interior in regions where the depth of the mixed layer is not uniform. The relative contributions of vertical velocities due to Ekman pumping and lateral advection through a sloping mixed layer base to the overall subduction rate were considered by *Cushman-Roisin* [1987] and *Woods* [1985]. *Marshall et al.* [1993] (hereinafter referred to as MNW) have estimated the subduction rate in the eastern North Atlantic arising from each of these effects using climatological hydrography and wind stress curl fields.

The rate at which water is subducted into the main thermocline is intimately related to the thermodynamics of the upper ocean [*Nurser and Marshall*, 1991; MNW; *Marshall and Marshall*, 1995, hereinafter referred to as MM95]. In order for a parcel to be subducted below the mixed layer the near-surface waters must be restratified. This change in buoyancy of the near surface may be achieved by heat exchange with the atmosphere, lateral advection by the large-scale flow, or lateral advection by mesoscale eddies. The relative influences of these

components can be expected to depend strongly on the dynamical regime and nature of the seasonal cycle. Thus, while one can calculate the subduction rate from the kinematic relationship between the velocity field and the mixed layer depth, much of the insight into what determines the subduction rate is revealed by understanding the three-dimensional upper ocean heat budget that controls the seasonal cycle of the upper ocean stratification and mixed layer depth.

The relative contributions of geostrophic advection, Ekman transport, mixing, surface fluxes, and eddy fluxes to the upper ocean heat budget are difficult to determine directly from observations. The annual mean heat budget is achieved by a balance of terms whose high-frequency variability is much larger than their annual mean. For example, the seasonal cycle in heat flux is an order of magnitude larger than the annual mean, while the relatively high-frequency lateral advection of temperature due to mesoscale eddies is an order of magnitude larger than the large-scale advection. The spatial and temporal coverage required to estimate these terms from observations is prohibitive.

This paper is the third in a series of papers in which data collected by the Subduction Experiment moorings and hydrography are studied in the context of the subduction process. In the first paper, R. A. Weller et al. (The large-scale context for oceanic subduction in the northeast Atlantic, submitted to *Journal of Geophysical Research*, 2000, hereinafter referred to as Weller et al., submitted manuscript, 2000) describe the 2 year time series of meteorological forcing and upper ocean variability and explore the extent to which the upper ocean response can be explained by local atmospheric forcing. The second paper, by P. Furey et al. (Simulations of mixed layer response to local atmospheric forcing and inferring the subduction rate in the northeast Atlantic, submitted to *Journal of Geophysical Research*, 2000, hereinafter referred to as Furey et al., submitted manuscript, 2000), evaluates three one-dimensional mixed layer models for their ability to simulate the evolution of the upper ocean stratification at the mooring locations over the 2 year time period. The best performing of these three models is then used to calculate the mixed layer depth over the eastern subtropical gyre, which, together with climatological hydrography and the gridded wind stress data, is used to estimate the subduction rate during the Subduction Experiment.

In the present study the output from a three-dimensional general circulation model is used to diagnose the upper ocean heat budget in the eastern North Atlantic. The purposes of this study are twofold: (1) to explore the thermodynamic balances in the seasonal thermocline and their impact on the subduction rate and (2) to evaluate the seasonal cycle in SST and upper ocean stratification from a large-scale climate model forced with surface flux data. The observed evolution of the upper ocean thermal structure on large scales over the 2 year time period of the Subduction Experiment provides a unique opportunity to benchmark the realism of the model simulation in this region. The model fields then provide a means to diagnose and decompose the upper ocean heat balances and to expose the important contributions resulting from processes that would be very difficult to observe directly in the ocean. In this way we make use of both the observations and the model physics to explore the upper ocean balances.

The paper is outlined as follows. A brief summary of the model is given in section 2. Comparisons made between the model upper ocean temperature, mixed layer depth, and sur-

face fluxes and direct measurements taken at five moorings as part of the Subduction Experiment are given in section 3. The model heat budget in the upper ocean of the subtropical gyre is presented in section 4. Estimates of the subduction rate over the eastern North Atlantic during the period of the Subduction Experiment (June 1991 through June 1993) made from the model fields using both kinematic and thermodynamic methods are given in section 5. Finally, a summary and conclusions are given in section 6.

2. Model Description

The model used in this study is the National Center for Atmospheric Research (NCAR) Climate System Model (CSM) Ocean Model. Only a brief discussion of the model formulation and subgridscale parameterizations is included here. More complete discussions are given by *Large et al*. [1997, and reference therein] and *Gent et al*. [1998, and references therein]. The model solves the primitive equations of motion in a global domain with coarse representations of all the major topographic features. The lateral resolution is a uniform 3.6° in longitude and varies in latitude between 1.8° near the equator and 3.4° at midlatitudes and then decreases as the cosine of latitude to a minimum of 1.8° poleward of 60°N. There are 25 levels in the vertical monotonically increasing in thickness from 12 m near the surface to 450 m near the bottom. Subgridscale mixing is parameterized with a horizontal eddy viscosity of $A_{MH} = 3 \times 10^5$ m^2 s^{-1}, an isopycnal diffusion of $A_I = 0.8 \times 10^3$ m^2 s^{-1}, and an isopycnal thickness diffusion of $A_{ITD} = 0.8 \times 10^3$ m^2 s^{-1}. The horizontal diffusion of tracers (along constant depth) is set to zero.

The model is based on the Geophysical Fluid Dynamics Laboratory MOM 1.1 z coordinate model; however, it incorporates several different physical parameterizations and numerical integration schemes. The influences of unresolved mesoscale eddies on the transport of temperature and salinity along isopycnal surfaces are parameterized using the scheme of *Gent and McWilliams* [1990]. This approach, when used together with zero horizontal diffusion, has been found to result in several improvements in the large-scale hydrography and water mass characteristics in noneddy-permitting ocean models, as described by *Danabasoglu and McWilliams* [1995].

The vertical mixing in the upper ocean is represented by the K profile parameterization (KPP) scheme documented by *Large et al*. [1994]. The mixing of momentum and tracers due to internal wave breaking (uniform with depth) and shear instabilities (gradient Richardson number dependence) is parameterized as downgradient fluxes. The mixing coefficients vary with depth within the boundary layer and may even result in significant penetration of strong mixing into the stratified region beneath the traditional weakly stratified "mixed layer." The model also parameterizes the nonlocal transport of tracers under unstable density profiles because of turbulent eddies in the mixed layer. The mixing coefficients and their vertical derivative are matched with those in the interior at the base of the turbulent boundary layer. Additional details of the mixing scheme and its implementation in a general circulation model are given by *Large et al*. [1997].

The model is forced at the surface with fluxes of momentum, heat, and fresh water. The turbulent heat fluxes are calculated from basic atmospheric variables using bulk formulas. The required surface winds, air temperature, and air humidity are obtained from the National Centers for Environmental Pre-

diction (NCEP) global reanalysis data set. The NCEP reanalysis also provides the surface wind stress. Cloud fraction is provided by *Rossow and Schiffer* [1991], and surface insolation is obtained from the International Satellite Cloud Climatology Project (ISCCP). The downward shortwave flux is allowed to penetrate into the ocean such that one third of the flux penetrates with an *e*-folding depth of 17 m. The surface insolation of ISCCP was uniformly reduced by 12.5%, and the NCEP air humidity was reduced by 7% in order to balance the global heat budget [see *Large et al.*, 1997].

The precipitation at the surface required for the net freshwater flux into the ocean was computed from the microwave sounding unit [*Spencer*, 1993]. The precipitation was multiplied by a factor such that the global precipitation balanced the global evaporation. In order to minimize global drifts further and to represent river runoff crudely the sea surface salinity was restored toward the Levitus climatology with a timescale of 6 months.

The model was spun up for 270 years with a repeat application of forcing derived from the NCEP reanalysis products for the 24 year period 1973–1996. There was also an acceleration of the time step below 1000 m such that the deep ocean was integrated for 13,500 years. The atmospheric state variables and surface fluxes are provided every 6 hours. The cloud cover and solar insolation data sets are available only between July 1983 and June 1991; a mean monthly climatology is used for other years. The model was integrated synchronously (no deep acceleration) for an additional 15 years using the same forcing data set for 1978 through the end of 1993. The analysis in the present paper is confined to the period of the Subduction Experiment, June 1991 through June 1993 of this final 15 years of synchronous integration.

A summary of the mean flux components measured at the moorings is given in Table 1 (note that these are not annual mean fluxes). There is a net heat flux into the ocean at each of the mooring locations, with a maximum heating rate of nearly 40 W m^{-2} at the central mooring (CE) and southeast mooring (SE) locations. Cooling is dominated by latent heat flux and the net long wave outgoing heat flux. Sensible heat fluxes are small and slightly negative at each of the moorings. The accuracy of the mean values from the buoy data were estimated by *Moyer and Weller* [1997] to be ±2 W m^{-2} for SHF; ±15 W m^{-2} for LHF; ±6 W m^{-2} for NSW; and ±15 W m^{-2} for NLW. The errors do not sum constructively, and the error in NHF is estimated to be ∼±16 W m^{-2}. This conclusion is substantiated

Table 1. Average Heat Flux Components at the Five Mooring Locations[a]

Mooring (latitude, longitude)	SHF	LHF	NSW	NLW	NHF
NW (34°W, 33°N)	−6.5	−91.8	186.0	−73.6	14.1
NE (22°W, 33°N)	−9.2	−96.4	185.6	−66.1	13.8
CE (29°W, 25.5°N)	−6.3	−106.0	211.8	−60.9	38.6
SW (34°W, 18°N)	−4.4	−127.3	216.4	−61.4	23.3
SE (22°W, 18°N)	−7.1	−103.3	200.0	−51.2	38.4

[a]Positive values indicate heat flux into the ocean (W m^{-2}). Abbreviations are SHF, sensible heat flux; LHF, latent heat flux; NSW, net short wave heat flux; NLW, net long wave heat flux; and NHF, net heat flux. The averaging periods are NW, July 4, 1991, to May 31, 1993; NE, June 19, 1991, to June 13, 1993; CE, June 23, 1991, to June 15, 1993; SW, June 26, 1991, to June 20, 1993; SE, June 29, 1991, to June 18, 1993.

Table 2. Average Heat Flux Components From the Model With NCEP-Based Fluxes Interpolated to the Mooring Locations[a]

Mooring	SHF	LHF	NSW	NLW	NHF
NW	−9.9	−90.9	159.6	−55.2	3.6
NE	−10.2	−86.1	157.4	−56.4	4.7
CE	−10.7	−114.8	194.9	−65.0	4.4
SW	−10.9	−133.0	202.6	−61.5	−2.8
SE	−13.9	−131.5	204.1	−66.3	−7.6

[a]Positive values indicate heat flux into the model ocean (W m^{-2}). Abbreviations are SHF, sensible heat flux; LHF, latent heat flux; NSW, net short wave heat flux; NLW, net long wave heat flux; and NHF, net heat flux. The model fluxes have been averaged over the same period as the mooring fluxes in Table 1.

by agreement between the buoy average net heat flux data and coincident 2° by 2° box averages from the Southampton Oceanography Centre flux to within 10 W m^{-2} [*Josey*, 2000]. A detailed discussion of the observed heat fluxes at the mooring locations and a comparison between the measured surface fluxes and flux estimates derived using basic observables from various numerical weather prediction models and bulk formula are given by *Moyer and Weller* [1997].

The mean heat flux components from the model interpolated to the mooring locations are given in Table 2 (note that these are not annual mean fluxes). The model sensible heat flux is similar to, but generally slightly more negative than, each of the mooring estimates. For the other flux components the differences between the model and observed heat fluxes are generally much smaller than the average flux over the 2 year simulation. Perhaps most important for the overall upper ocean heat budget is the net heat flux into the ocean. The net flux into the model ocean is less than is observed at each of the moorings by between 9.1 and 46 W m^{-2}. The 95% confidence limits on the buoy net heat flux, based on estimates done for each season by *Moyer and Weller* [1997], is ±16 W m^{-2}. The closest agreement is found for the two northern locations. At the two southern locations the net heat flux into the model ocean is of the wrong sign.

A clearer picture of the net heat flux into the model ocean over the eastern North Atlantic is given by the mean net heat flux over the 2 year integration, as shown in Figure 1a. The horizontal velocity field at 93 m depth in Figure 1b shows clearly the anticyclonic circulation of the wind-driven subtropical gyre, with stronger velocities in the northwest corner near the Gulf Stream. There is a net heat flux into the ocean over most of the eastern subtropical gyre. There is strong heat loss in the northwest corner over the relatively warm Gulf Stream. No mooring data are available there, but this is consistent with the expected sign of the net heat flux [*Isemer and Hasse*, 1987]. There is also weak cooling in the southern portion of the domain where the mooring flux data indicate heating. The *Isemer and Hasse* [1987] climatology also indicates weak cooling between 10° and 20°N of $O(10$ W m$^{-2})$; however, it is largely confined to the region to the west of 25°W. The cooling due to latent heat flux in the model in this region is much stronger than is estimated by the mooring measurements, particularly the southeast mooring.

3. Model-Data Comparison

The monthly mean upper ocean temperature and stratification in the model are compared to that observed at the five
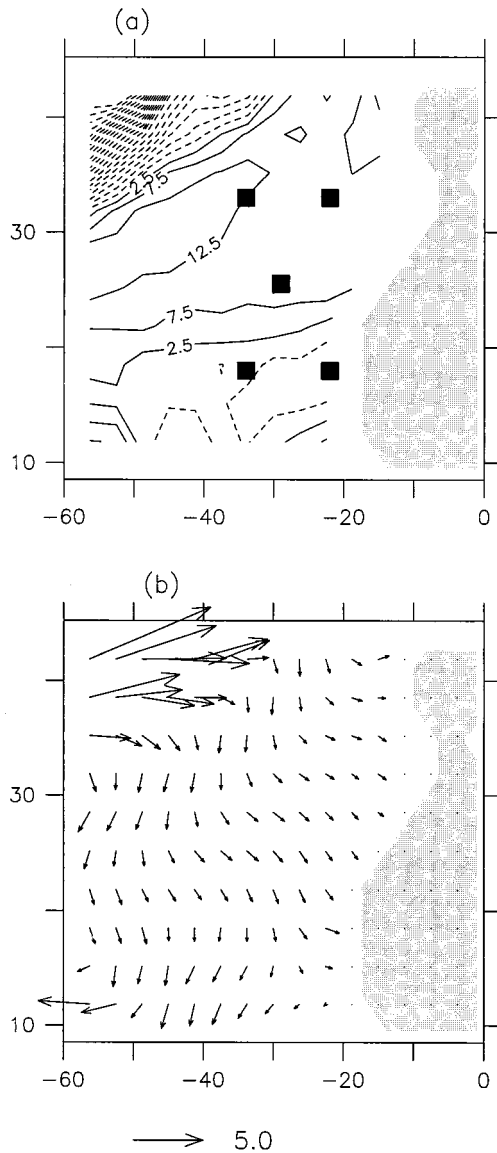
Figure 1. (a) Mean heat flux into the model ocean over the 2 year period of the Subduction Experiment, June 1991 through June 1993 (W m^{-2}). Positions of the Subduction Experiment moorings are indicated by the symbols. (b) Mean horizonal velocity at 93 m depth (cm s^{-1}).

ment between the model and observations. The seasonal cycle varies between about 8°C in the north and 4°C in the south. The model does a reasonably good job of reproducing the seasonal cycle at each of the mooring locations, although the model is systematically too warm at the southeast mooring. While the interannual variability is small compared to the seasonal cycle, the model is also able to reproduce some of these observed features as well (cool summer of 1992 at CE, northeast mooring (NE), and northwest mooring (NW) location. The mean difference between the modeled and observed SSTs at all of the moorings is 0.2°C with a standard deviation of 0.5°C.

The depth to which the upper ocean temperature is mixed vertically combined together with the evolution of SST provides a useful diagnostic for the upper ocean stratification. While there are many ways to define the depth over which
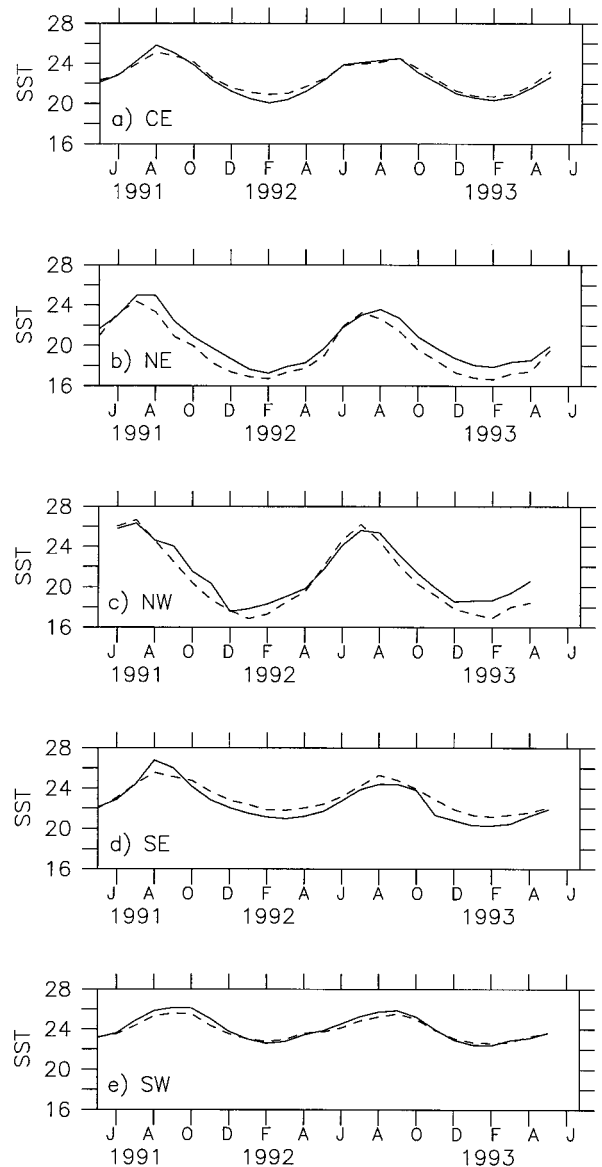
mooring locations for the 2 year period June 1991 through June 1993. Data at the mooring locations are obtained from nearby ship of opportunity data for periods in which the moorings had failed. Details of how the data gaps have been filled and a comparison with independent measurements at the mooring locations are given by Weller et al. (submitted manuscript, 2000). The primary focus of the present study is on the maintenance and seasonal to interannual variability of the upper ocean heat budget, so the higher-frequency variability associated with individual atmospheric events are filtered out by averaging into monthly means. A discussion of the local atmospheric forcing of high-frequency events is given by Furey et al. (submitted manuscript, 2000).

The sea surface temperature (SST) at the five mooring locations is shown in Figure 2 for the observations (solid line) and the model (dashed line). There is generally good agree-

Figure 2. Comparison of the monthly mean SST (°C) for the model (dashed line) and the mooring observations (solid line) for the period June 1991 through June 1993 interpolated to the (a) central, (b) northeast, (c) northwest, (d) southeast, and (e) southwest mooring locations.

vertical mixing is strong, we use a simple criterion of a change in temperature of 0.5°C relative to the surface temperature so that direct comparisons can be made between the model and the mooring observations (which did not measure salinity). The diagnosed mixed layer depth (MLD) at the five mooring locations is shown in Figure 3 for the observations (solid line) and the model (dashed line). The mixed layer depth varies from <20 m in the summer to a maximum of >150 m at the northeast mooring in winter. The seasonal cycle is reasonably well reproduced by the model at most mooring locations, with the exception of the southeast mooring. Aspects of the inter-annual variability are also reproduced by the model, such as the deepening of the winter mixed layer in 1992–1993 at the northeast mooring, although the deep mixed layers at NW and southwest mooring (SW) location during the 1991–1992 winter
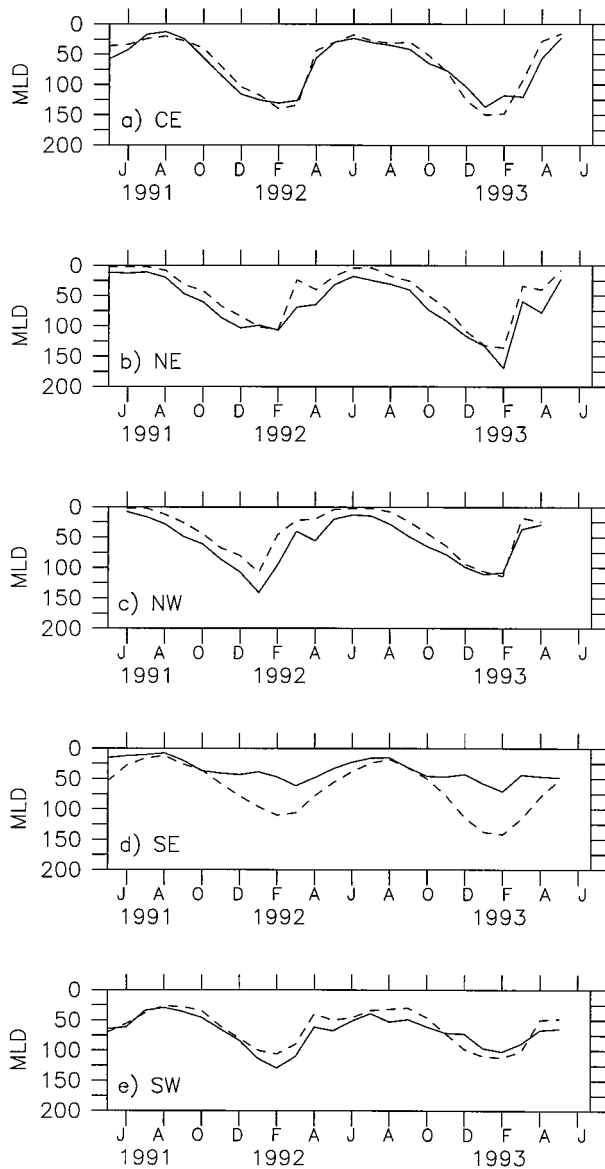
Table 3. Average Heat Flux Components From the Model With ECMWF-Based Fluxes Interpolated to the Mooring Locations[a]

Mooring	SHF	LHF	NSW	NLW	NHF
NW	4.4	−166.1	202.2	−72.2	−31.7
NE	−6.2	−110.2	191.9	−74.9	0.6
CE	−12.8	−134.8	229.2	−71.6	10.0
SW	−13.6	−152.8	243.3	−66.9	10.0
SE	−10.3	−149.0	216.5	−63.4	−6.2

[a]Positive values indicate heat flux into the model ocean (W m^{-2}). Abbreviations are SHF, sensible heat flux; LHF, latent heat flux; NSW, net short wave heat flux; NLW, net long wave heat flux; and NHF, net heat flux. The model fluxes have been averaged over the same period as the mooring fluxes in Table 1.

are missed. The mean difference between the modeled MLD and the observed MLD at all five moorings is −3 m, with a standard deviation of 15 m.

The warm SST and deep MLD in the model at the southeast mooring is a result of the basic stratification in the model being much too strong here. The cause of this error is unknown but may be related to the transition from a region of Ekman pumping in the subtropical gyre interior (where all four other moorings are located) to a region of Ekman suction near the tropical/subtropical gyre boundary. This is also a region where the winds are offshore, resulting in both coastal upwelling and large atmospheric transports of dust over the ocean. Interestingly, the model net heat flux is much too weak here, yet the SST is too warm. This suggests that the model is missing a source of cooling from within the ocean. The primary focus here is on the heat budget of the subtropical gyre, so most of the analysis will focus on the region clearly contained within the subtropical gyre.

A second model integration was carried out in which the atmospheric heat and freshwater fluxes were derived from the European Center for Medium-Range Weather Forcasting (ECMWF) weather model. *Moyer and Weller* [1997] found generally slightly better agreement between the mooring flux estimates and those calculated using the ECMWF basic observables rather than the original NCEP observables (not the reanalysis product used to force the present model). The second model simulation using the ECMWF-based fluxes provides a test of the sensitivity of the model simulations to variations in the surface fluxes that are within the uncertainties of the reanalysis products. The average fluxes at the mooring locations based on the ECMWF basic observables are not appreciably better than those for the NCEP based run (Table 3). The net heat flux into the ocean compares better with the mooring estimates at three locations and worse at two locations. The net heat flux into the model ocean is still less than the mooring estimates at all mooring locations. Differences between individual flux components tend to be larger than the differences in the net flux, with compensation occuring between increased short wave flux being balanced by increased cooling due to the latent heat flux and, to a lesser degree, long wave radiation. The underestimate of the net heat flux into the model ocean based on the meteorological observables from both the NCEP reanalysis and the ECMWF reanalysis is consistent with the findings of *Josey* [2000], where net heat flux from both reanalysis products was found to underestimate the net heat flux into the ocean compared to that measured at the buoys.
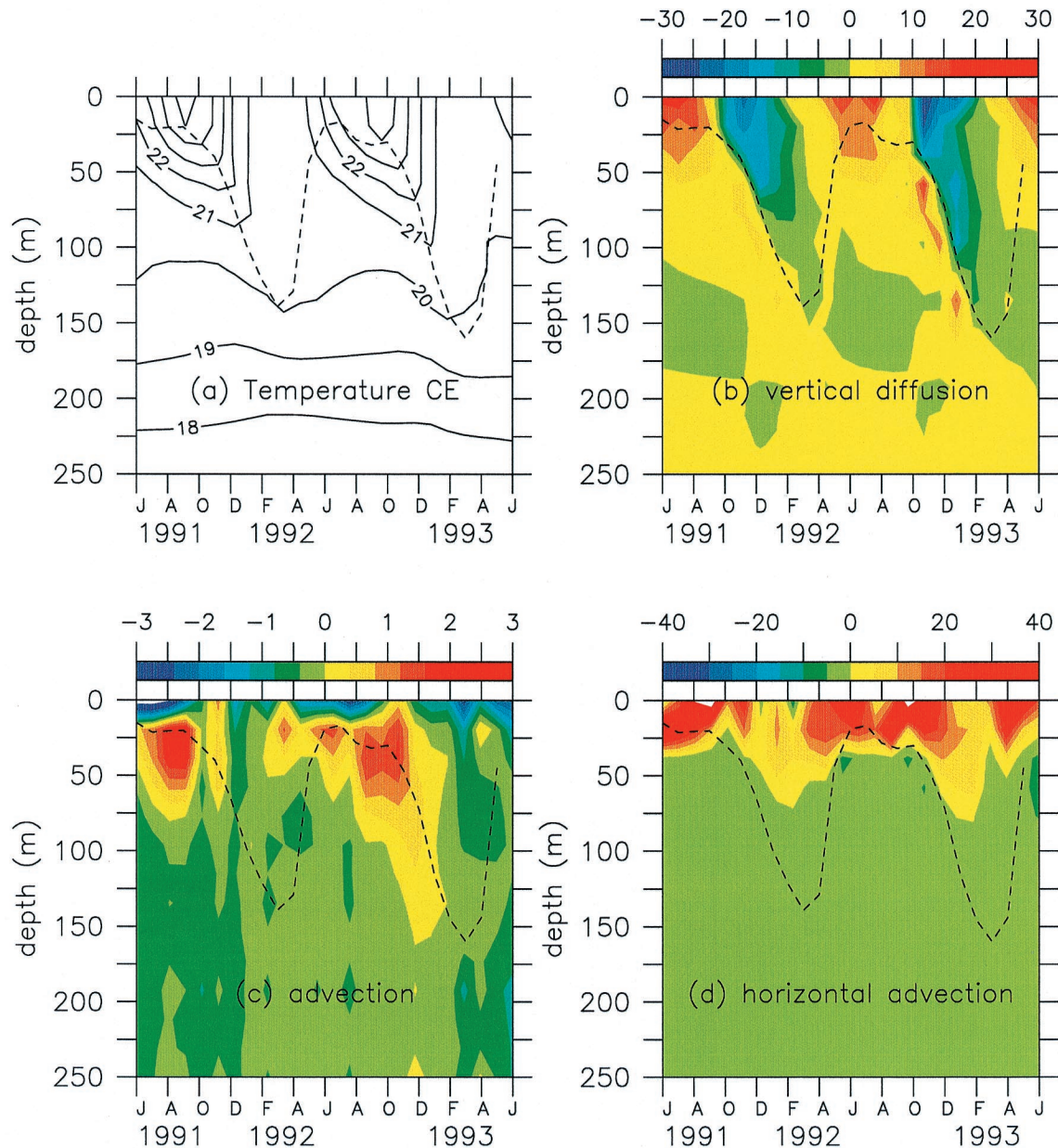

Figure 3. Comparison of the monthly mean mixed layer depth (in m, temperature 0.5° less than SST) for the model (dashed line) and mooring observations (solid line) for the period June 1991 through June 1993 interpolated to the (a) central, (b) northeast, (c) northwest, (d) southeast, and (e) southwest mooring locations.

Plate 1. Upper ocean evolution of (a) temperature (°C), and the time rate of change of temperature due to (b) vertical diffusion, (c) advection, (d) horizontal advection, (e) vertical advection, (f) eddy advection (parameterized), and (g) along-isopycnal diffusion for the period June 1991 through June 1993 (°C yr^{-1}) at CE. The dashed line indicates the MLD.

The model simulation of SST and MLD is very similar to that of the control case shown in Figures 2 and 3 and is not shown here. The model mean error and standard deviations are similar to but slightly worse than those for the NCEP-based calculation. The average modeled SST is 0.24°C warmer than the moorings, with a standard deviation of 0.8°C. The MLDs are on average 4 m shallower than the moorings with a standard deviation of 34 m.

A consistent ECMWF-based data set was produced only for the eastern North Atlantic. The application of this alternate forcing data set to the global ocean model results in unrealistic gradients in the flux and upper ocean thermal structure at the edges of the region where the modified forcing is applied. Thus, while this model run is useful at diagnosing the sensitiv-

ity of the modeled upper ocean thermal structure at the mooring locations, it is not appropriate for the basin-scale analysis that is the focus of the remainder of the paper. The dominant balances at each of the mooring locations was found to be the same in both model runs, so the conclusions regarding the basic thermal balances are not changed.

Although both model calculations compare reasonably well with the observations, the result that the modeled SST compares very well with the mooring measurements while the model surface heat fluxes are systematically too low suggests that the model stratifies the upper ocean too strongly. This may be a result of inadequate vertical mixing, weak lateral advection, or an overestimate of the restratification due to mesoscale eddies.
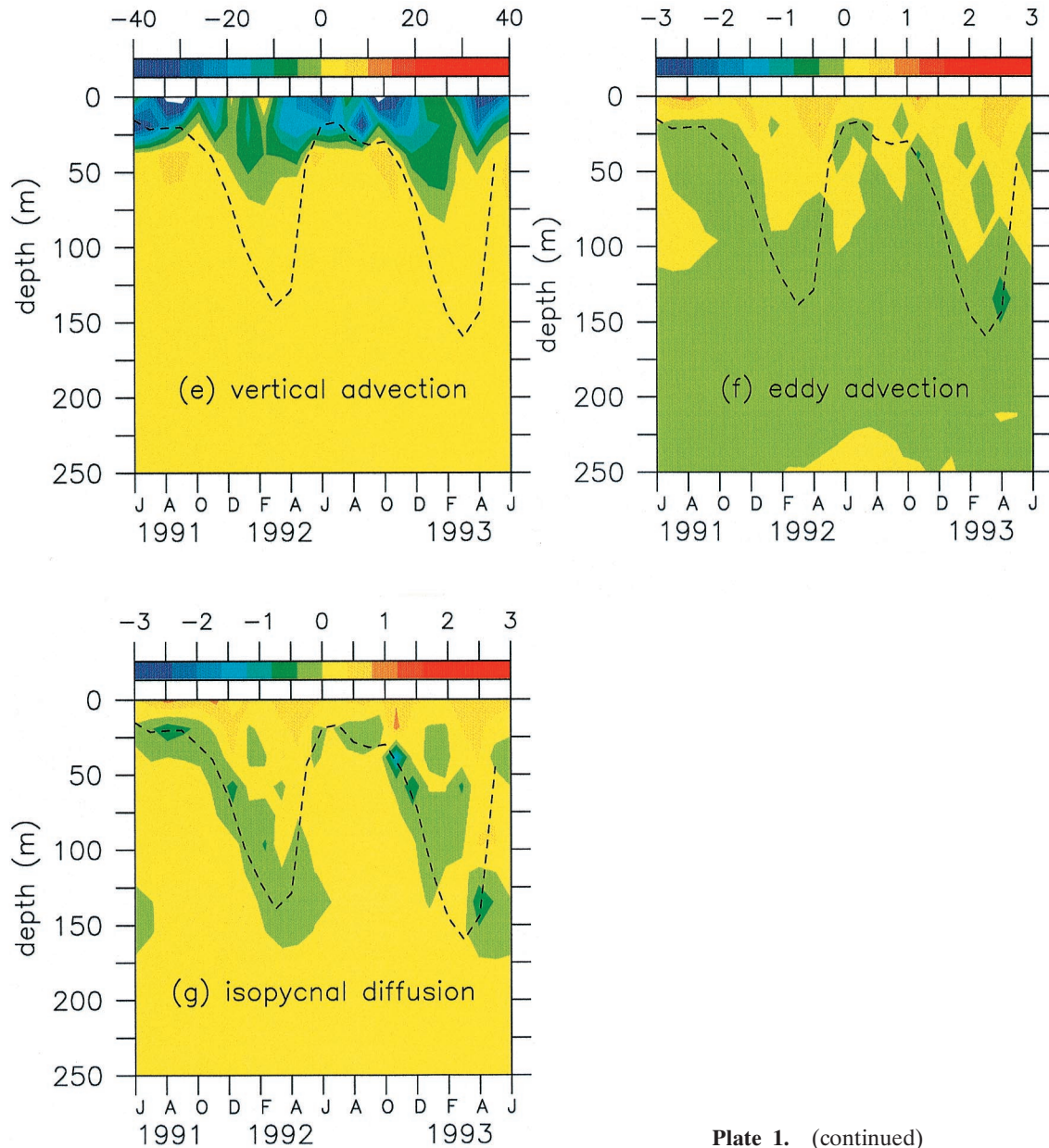
Plate 1. (continued)

Calculations with one-dimensional vertical mixing models (including the KPP model used in the National Center for Atmospheric Research (NCAR) (CSM) ocean model) that were initialized with observed temperature profiles and forced with the observed fluxes diverged from the observed SST and MLD by more than the model errors reported here in only 1–2 months integration time (Furey et al., submitted manuscript, 2000). Therefore, even though the model is very low resolution and does not accurately represent many small-scale features (such as the Azores Current), we believe that the three-dimensional model physics are a realistic and essential component of the upper ocean heat budget.

4. Model Upper Ocean Heat Budget

The close agreement between the model and the observations in both the SST and MLD suggests that the model may provide useful insights into the maintenance of the upper ocean stratification and evolution of the seasonal pycnocline. The model fields provide a dynamically and thermodynamically consistent four-dimensional data set from which one can diagnose the relative importance of various terms in the local heat budget.

The heat balance at the central mooring region is diagnosed as a function of depth and time from the model prognostic equation for temperature

$$\frac{\partial T}{\partial t} = -\frac{1}{a \cos \phi} \underset{A}{[(u + u^*)T]_\lambda} - \underset{A}{[(v + v^*)T]_\phi}$$

$$- \underset{B}{[(w + w^*)T]_z} + \underset{C}{R(\kappa_I, T)} + \underset{D}{[\kappa_V(T_z} - \underset{E}{\gamma_T)_z} + \underset{F}{H.} \quad (1)$$

The terms on the right-hand side represent lateral advection (A), vertical advection (B), along isopycnal diffusion (C), vertical diffusion (D), and penetrating solar radiation (E) and

latent heating due to sea ice formation (F; zero in the region of interest). Longitude is indicated by λ, latitude is indicated by ϕ, and subscripts denote partial differentiation. The term γ_T is a nonlocal transport term in the KPP boundary layer mixing model. It is nonzero only for tracers under unstable (convective) forcing. In addition to the zonal, meridional, and vertical velocities, the advection operator contains additional advection by an eddy-induced transport velocity (u^*, v^*, w^*) defined as

$$u^* = \left(\frac{A_{\mathrm{ITD}}}{a \cos \phi} \frac{\rho_\lambda}{\rho_z} \right)_z, \qquad v^* = \left(\frac{A_{\mathrm{ITD}}}{a} \frac{\rho_\phi}{\rho_z} \right)_z$$

$$w^* = -\left(\frac{1}{a \cos \phi} \right) \left[\left(\frac{A_{\mathrm{ITD}}}{a \cos \phi} \frac{\rho_\lambda}{\rho_z} \right) + \left(\frac{A_{\mathrm{ITD}} \cos \phi}{a} \frac{\rho_\phi}{\rho_z} \right)_\phi \right], \qquad (2)$$

where ρ is the potential density and A_{ITD} is the isopycnal diffusivity. The reader is referred to *Large et al.* [1997, and references therein] for details on the above parameterizations and numerical solution procedure.

4.1. Subtropical Gyre Interior

The central mooring is in a region of Ekman pumping far from strong boundary currents. The general balances obtained here are representative of the subtropical gyre interior. The horizontal variations in the dominant heat budget terms will be discussed in the following section.

The temperature at the central mooring location as a function of time and depth is shown in Plate 1a. The seasonal cycles in SST and MLD are clearly indicated. The MLD shown here was calculated as the depth at which the buoyancy differs from the surface buoyancy by 3×10^{-4} m s^{-2} [*Large et al.*, 1994]. This includes saline effects and differs only slightly from the MLD shown in Figure 3, which was based on temperature only for comparison with the mooring observations. The terms that contribute to the time rate of change of temperature are shown in Plates 1b–1g.

The seasonal cycle is dominated by the vertical diffusion term (Plate 1b), which includes the surface heat flux, the penetrative short wave insolation, and the vertical mixing due to both convection and local mixing (note the change in scale between Plate 1b and Plates 1c, 1f, and 1g). Warming in spring and summer restratifies the upper ocean. This warming trend is diffused downward in time through the winter, even as the upper ocean is being cooled and the mixed layer is deepening. The deep warming finally ceases when warming and restratification begin near the surface in the following spring. The reverse is true in summer: the cold waters that are formed in the previous winter/spring continue to be diffused downward throughout the summer months, cooling the deep seasonal thermocline. As will be shown in Figure 4, the net effect of vertical mixing is to warm the ocean below the deepest extent of convective mixing.

The net change in temperature due to advection by the large-scale flow is shown in Plate 1c. The relative influences of horizontal advection and vertical advection are shown in Plates 1d and 1e (note the change in contour interval). The net advection tends to decrease the temperature near the surface, increase the temperature just below the surface, and cool the ocean below the depth of the seasonal pycnocline.

At the surface, horizontal heat flux convergence tends to increase SST as a result of the convergent Ekman transport. The vertical heat flux convergence works to decrease SST by advecting this warm water vertically (the vertical flux divergence is always negative because the vertical velocity at the surface is zero). The net effect of advection will depend on the relative influences of horizontal convergence (warming) and vertical divergence (cooling). We find that the net effect of advection at the central mooring location is to cool the surface layer.

The net effect of advection in the seasonal pycnocline (25–75 m) is warming (Plate 1c). This happens largely as a result of the vertical advection of warm SSTs downward out of the shallow mixed layer in summer (Plate 1e). There is a slight cooling effect in winter, also due to vertical advection, but the vertical gradients in summer are sufficiently stronger, so that the net effect integrated over an annual cycle is warming. The importance of Ekman pumping and the seasonal cycle of mixed layer depth in the upper ocean heat budget and, by implication, in the overall subduction rate was noted by J. M. Federiuk and J. F. Price (unpublished manuscript, 1985), MNW, and MM95. The deep ocean below the seasonal pycnocline experiences cooling due to lateral advection of cold waters from the north by the large-scale subtropical gyre circulation.

Lateral subgridscale processes are parameterized by a temperature flux due to unresolved mesoscale eddies (Plate 1f) and an along-isopycnal diffusion of temperature (Plate 1g). The eddy advection term tends to restratify the upper ocean weakly, as expected for a parameterization of eddies generated by baroclinic instability of the local, large-scale flow. The eddy fluxes are active all year round but are strongest in winter when SST gradients are the largest and baroclinic instability would be expected to be most active. The along-isopycnal diffusion also weakly restratifies the upper ocean and is most active in winter. Diffusion tends to warm the near-surface water and, to a lesser degree, the deep ocean.

The net influences of each of these terms in the maintenance of the mean upper ocean stratification is best summarized by the annual average of the terms in Plates 1b–1g, as shown in Figure 4. Vertical diffusion of heat through the surface into the ocean acts to warm the near surface (short dashed line), as does the restratification due to parameterizations of eddy fluxes and along-isopycnal diffusion. This warming is balanced by cooling due to vertical advection. The balance in the seasonal pycnocline (25–75 m) is between warming due to advection (primarily due to Ekman pumping in summer) and vertical diffusion (which includes winter time convection). While the amplitude of the advective term is $O(1°C \ yr^{-1})$, much less than the seasonal variability in the surface flux/vertical diffusion term, there is much less cancelation on the seasonal timescale so that it is of leading order in the annual mean. The warm water pumped down in summer is diffused from the seasonal pycnocline to the deep waters (depth >100 m) from summer through to the end of winter. The deep balance below the seasonal pycnocline is primarily between this vertical and along-isopycnal diffusion of heat and lateral advection of cold water from the north.

4.2. Balances Over the Eastern North Atlantic

The relative influences of advection and diffusion in the maintenance and evolution of the seasonal pycnocline vary with location within the subtropical gyre. The annual mean horizontal velocity at 6 m depth is shown in Figure 5a. The central and low latitudes are dominated by the Ekman velocity of $O(5 \ cm \ s^{-1})$. The horizontal convergence is evident
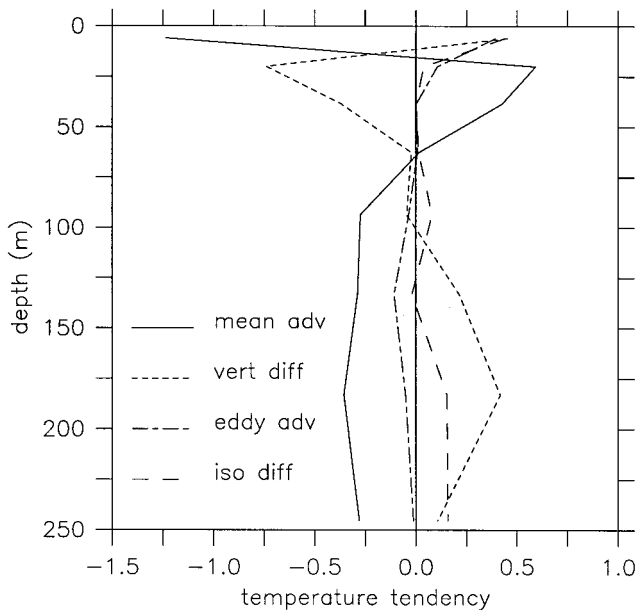
Figure 4. Time average of the temperature tendency terms versus depth at CE. The near surface is a balance between vertical advection (cooling) and vertical diffusion (surface heat flux), eddy fluxes, and along-isopycnal diffusion (heating). The seasonal pycnocline is warmed by vertical advection (primarily Ekman pumping in summer) and is cooled by vertical diffusion. Below the seasonal pycnocline the balance is between lateral advection (cooling) and vertical and along-isopycnal diffusion. The units are °C yr^{-1}.

throughout the subtropical gyre. The eastward penetration of the Gulf Stream is seen in the northwest. The isotherms of the mean SST are primarily zonal with somewhat cooler temperatures found approaching the eastern boundary (Figure 5b). The temperature gradients increase to the northwest as the strong thermal wind of the Gulf Stream is encountered. The annual mean contributions to the change in SST for the dominant terms in the heat budget are shown in Figures 5c–5f.

Advection is found to decrease the SST over much of the central and northern portions of the region (Figure 5d), including at CE. This is due to the vertical heat flux divergence's slightly exceeding the horizontal heat flux convergence (Figures 5e and 5f). To the south and west, however, the net effect of advection is to increase SST. These regions tend to be areas of relatively shallow mixed layers and increased stratification at the base of the mixed layer. In these regions the heat flux convergence due to advection is diffused vertically below the mixed layer (Figure 5c).

The lateral subgridscale parameterizations act to warm the sea surface slightly throughout the eastern North Atlantic (not shown). Eddy fluxes are nearly uniform in the gyre interior and increase toward the Gulf Stream, where the lateral density gradient increases. Along-isopycnal diffusion is of similar amplitude in the interior and also increases somewhat toward the Gulf Stream. The net effect of these subgridscale processes on the upper ocean heat budget and the subduction rate is discussed further in section 5.

The balances within the seasonal pycnocline are most clearly indicated at the middepth of the maximum penetration of the mixed layer over the 2 year period. Figure 6a shows the horizontal velocity at the middepth of the seasonal pycnocline, and

Figure 6b shows the middepth of the seasonal pycnocline. The velocity north of ~18°N reflects the geostrophic flow of the main thermocline. However, the northward Ekman transport is clearly present at the middepth of the seasonal pycnocline at lower latitudes, a point which we return to in section 5. In the central subtropical gyre, lateral advection with the geostrophic flow (Figure 6e) is largely balanced by warming due to downward Ekman pumping in the summer (Figure 6f). This is the upper ocean heat gain following a Lagrangian column of fluid that contributes to subduction, as discussed by MNW and MM95. To the south, in the regions where the Ekman layer penetrates well into the seasonal pycnocline the balance is between net heating due to lateral heat flux convergence (which exceeds the vertical divergence) and cooling from vertical diffusion, the same as was found in the upper layer. In the Gulf Stream region, lateral advection of warm waters from the south is balanced by vertical diffusion downward.

Near the base of the seasonal pycnocline (not shown) the central subtropical gyre is cooled by lateral advection from the north. The cooling is largely balanced by vertical diffusion from the warmer surface layers above, as was discussed for the central mooring location. The influences of advection and diffusion are reversed near the Gulf Stream, where advection warms the region through lateral advection from the south while vertical diffusion carries this heat downward.

5. Subduction Rates

5.1. Kinematic Estimate of the Annual Subduction Rate

The rates at which fluid is subducted from the mixed layer into the permanent thermocline may be estimated kinematically by calculating the annual average mass flux through the surface defined as the maximum MLD over the 2 year period (h_{ml}) (MNW):

$$S = -w_{ml} - \mathbf{v}_{ml} \cdot \nabla h_{ml}. \quad (3)$$

The time-dependent term $\partial h/\partial t$ vanishes because h_{ml} is chosen as the maximum MLD over the 2 year period. This is preferable because it eliminates the possibility of reentrainment in the second winter. The average vertical and horizontal velocities at this depth are w_{ml} and $\mathbf{v}_{ml}$. Subduction is achieved by vertical advection at the base of the mixed layer and lateral advection in regions where the MLD is variable [Cushman-Roisin, 1987]. Marshall [1997] derived the subduction rate due to mesoscale eddies and showed that it may be represented as an eddy bolus velocity that interacts with the base of the mixed layer in much the same way as the Eulerian mean velocity to produce a net subduction due to mesoscale eddies. In the following analysis the total subduction velocities w_{ml} and $\mathbf{v}_{ml}$ are made up of contributions due to the large-scale advection by the Eulerian velocities and the bolus transport parameterization of the mass flux due to mesoscale eddies, as parameterized by Gent and McWilliams [1990].

This kinematic estimate is the most accurate means to calculate the subduction rate in the model. It is used here both to compare with previous estimates based on climatologies and to provide a benchmark for the approximate thermodynamic calculation that follows. Each of the terms in (3) has been calculated from the model fields. The maximum MLD is $O(100 \text{ m})$ over most of the subtropical gyre (Figure 7a). The deepening to the northwest as the Gulf Stream is approached is consistent with climatological MLDs (see, e.g., MNW); however, the
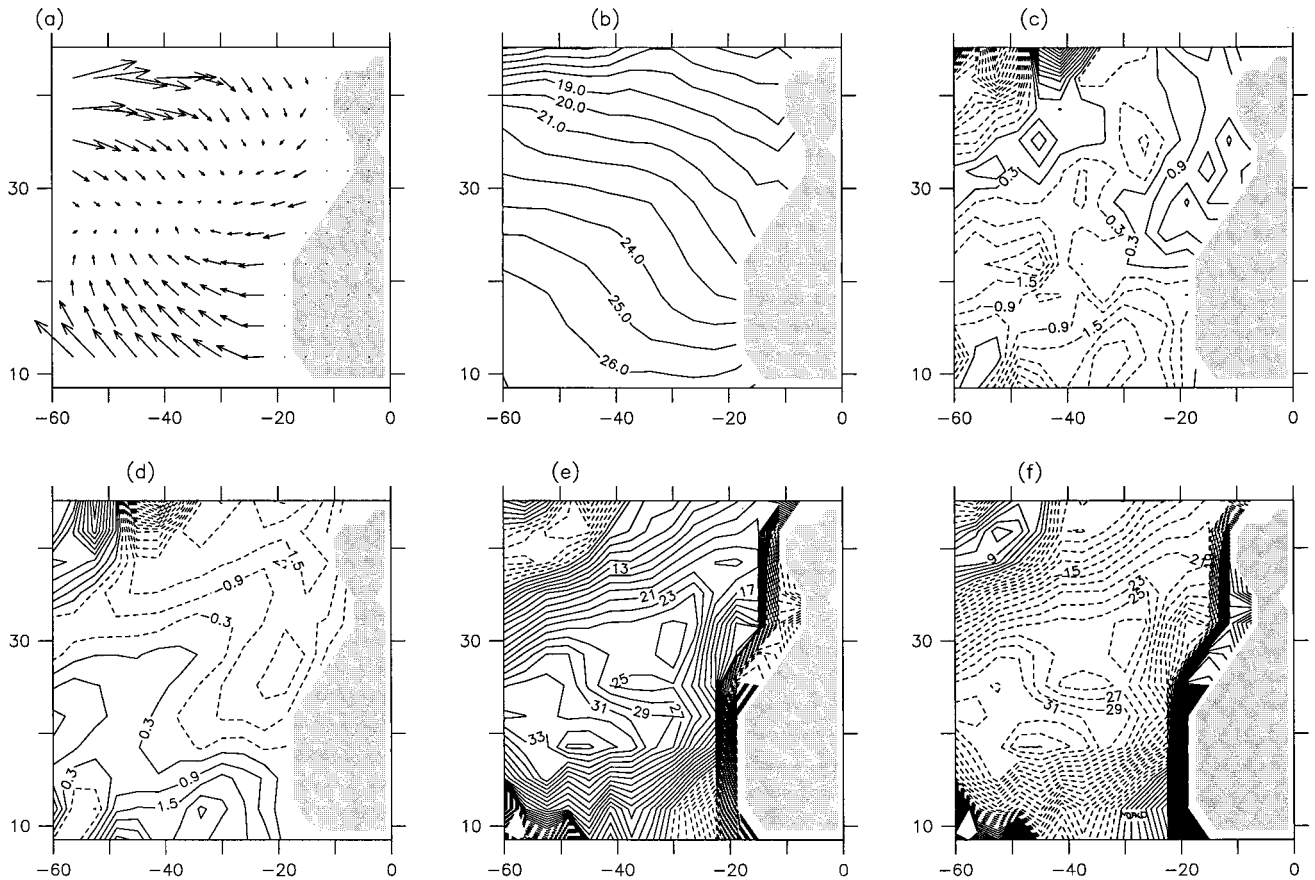
Figure 5. Time-averaged (a) velocity, (b) temperature (°C), and time rate of change of temperature due to (c) vertical diffusion, (d) advection, (e) horizontal advection, and (f) vertical advection at 6 m depth in the model (°C yr^{-1}).

deep mixed layers found near the eastern boundary are not seen in climatologies. This region of deep mixed layers is confined near the boundary and does not significantly affect the interior regions of interest here. There is a ridge of minimum MLD extending from 60°W, 20°N toward the northeast. A similar ridge was found in the higher-resolution model of *Williams et al.* [1995] and is also suggested in the data collected during the Subduction Experiment (Weller et al., submitted manuscript, 2000) and in the Levitus climatology (Furey et al., submitted manuscript, 2000).

The vertical advection at the base of the mixed layer is dominated by the mean Eulerian vertical velocity and reflects the Ekman pumping velocity (Figure 7b), although there is an increase to the south where the MLD shallows. The vertical velocity is downward over most of the subtropical gyre with magnitudes between 10 and 30 m yr^{-1}. The region of weak upwelling near 20°W, 30°N is not found in large-scale climatologies and is a result of a local region of Ekman diverence and upwelling during the period of the Subduction Experiment (Furey et al., submitted manuscript, 2000). The vertical velocity at the base of the mixed layer is $O(5-10$ m yr$^{-1})$ less than the Ekman pumping rate ($\sim$40 m yr^{-1} at the central mooring during this time period) because the meridional flow reduces the vertical velocity through the linear vorticity balance. There is upwelling in the northwest corner where the wind stress curl changes sign.

The lateral induction term shown in Figure 7c is also dom-

inated by the Eulerian mean velocities. There is large lateral advection out of the mixed layer in the northwest portion of the domain as it shallows to the south and east. Subduction is also positive where the mixed layer shallows south of 20°N. The ridge of minimum MLD results in lateral advection from the permanent thermocline into the winter mixed layer over the central subtropical gyre. A similar region of negative lateral subduction is found in the climatological analysis of MNW, although the amplitude is not discernable from the published figures.

The overall subduction rate estimated using (3) is shown in Figure 7d. Subduction is positive over most of the subtropical gyre with rates between 10 and 50 m yr^{-1}. Maximum rates exceeding 100 m yr^{-1} are found just south and east of the Gulf Stream where the mixed layer shoals rapidly to the southeast. This pattern and amplitude are similar to the kinematic estimate given by MNW. Common features include the strongly negative values within the Gulf Stream, large positive values just to the south of the Gulf Stream, a relative minimum in the eastern subtropical gyre, and increased values around 15°N. The subduction rate is near zero or slightly negative over much of the eastern subtropical gyre. The climatological analysis of MNW finds subduction of $O(50$ m yr$^{-1})$ over most of the central subtropical gyre. The rates found here are somewhat smaller primarily because of smaller values of the Ekman pumping calculated from the NCEP reanalysis. However, similarly low values are found using the ECMWF reanalysis
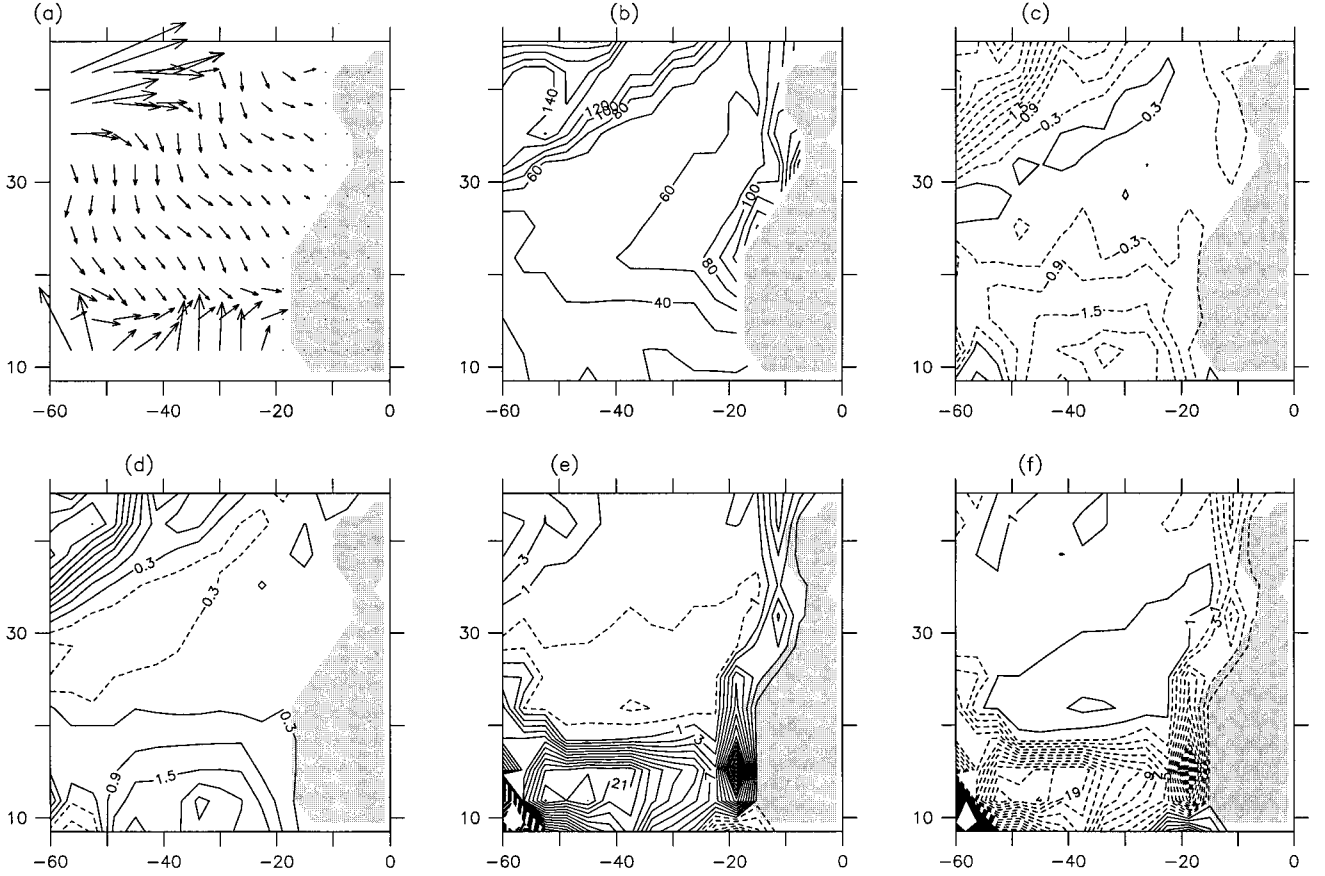
Figure 6. Time-averaged (a) velocity, (b) middepth of the seasonal pycnocline (m), and time rate of change of temperature due to (c) vertical diffusion, (d) advection, (e) horizontal advection, and (f) vertical advection at the middepth of the seasonal pycnocline in the model (°C yr^{-1}).

(Furey et al., submitted manuscript, 2000). Because both of these wind products compare well with the winds measured at the moorings during this period, it is believed that the low subduction rates calculated in this region during the period of the subduction experiment are a realistic deviation from the long-term subduction rate based on the climatological analysis of MNW.

5.2. Thermodynamic Estimate of the Annual Subduction Rate

Parcels are subducted from the winter mixed layer into the permanent thermocline through restratification of the upper water column over the seasonal cycle [*Nurser and Marshall*, 1991; MNW; MM95]. The net buoyancy flux supplied to the water column may be a result of surface fluxes, advection, or diffusion. Following *Nurser and Marshall* [1991] and MNW, the subduction rate may be related to the time rate of change of density following a column of water in the seasonal thermocline ($D\rho_m/Dt$) minus the time rate of change below the column in the permanent thermocline ($D\rho_T/Dt$) as

$$S = \frac{f(D\rho_m/Dt - D\rho_T/Dt)}{\rho_0 Q}. \tag{4}$$

The influences of a diabatic thermocline were included in the formulation of MNW but, for simplicity, were taken to be zero in their estimate of the subduction rate. MNW and MM95 relate the material derivative of the density following the geostrophic flow within the seasonal thermocline, and thus S, to the net buoyancy flux available for subduction H_{sub}:

$$S = \frac{\alpha f}{C_w h_{ml} Q} H_{\text{sub}}. \tag{5}$$

Here f is the Coriolis parameter, h_{ml} is the mixed layer depth, $Q = f \partial \rho / \partial z$ is the large-scale potential vorticity at the base of the seasonal thermocline, α is the thermal expansion coefficient of seawater, and C_w is the specific heat of seawater. MNW and MM95 relate the net buoyancy flux available for subduction to the net buoyancy flux at the surface and the wind-driven Ekman transport as

$$H_{\text{sub}} = \overline{H_{\text{net}}} - H_{\text{pump}}, \tag{6}$$

where the overbar denotes the annual mean. If the Ekman layer is assumed to be much thinner than the seasonal pycnocline, then the net buoyancy flux through the base of the Ekman layer, H_{net}, may be related to the buoyancy flux through the sea surface and the Ekman transport as

$$H_{\text{net}} = H_{in} + \frac{C_w}{\alpha} \mathbf{U_E} \cdot \nabla \rho_m, \tag{7}$$

where H_{in} is the net buoyancy flux through the surface, $\mathbf{U_E}$ is the horizontal Ekman transport, and ρ_m is the density in the mixed layer. The net buoyancy flux into the upper water column through the base of the Ekman layer may be quite different from the net buoyancy flux through the ocean surface as a result of lateral buoyancy flux by the Ekman transport.

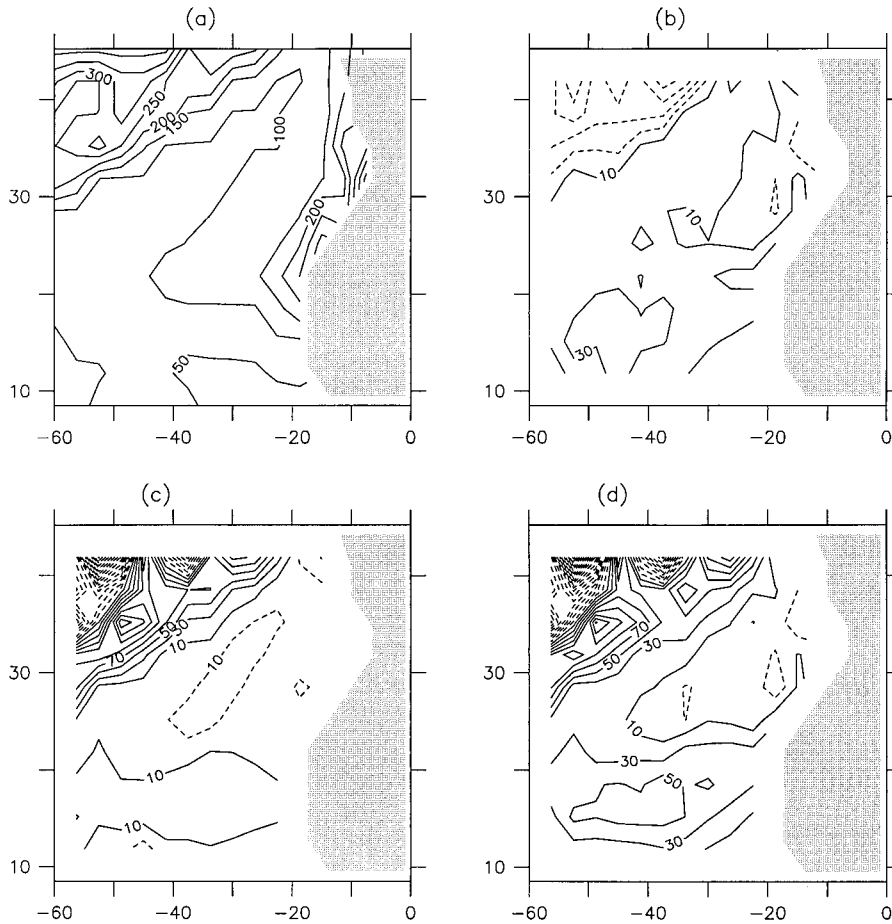H_{pump} is the buoyancy flux into the seasonal thermocline

Figure 7. Terms contributing to the kinematic estimate of the annual subduction rate: (a) maximum MLD (m), (b) time-averaged vertical velocity at the maximum MLD, (c) lateral induction terms, and (d) subduction rate (m yr^{-1}).

due to the vertical advection by the Ekman pumping velocity w_E. This may be expressed as the time integral of the seasonal Ekman pumping as

$$H_{\text{pump}} = \frac{C_w}{\alpha} \int w_E[\rho_s - \rho_m(t)]\, dt, \qquad (8)$$

where ρ_s is the density at the base of the seasonal thermocline. This contribution from Ekman pumping is taken as the annual average because the effective subduction period is very short over most of the subtropical gyre (MNW) and the stratification at the base of the mixed layer is weak during this time. MM95 show that for seasonal cycles in which the effective subduction period is very short, as is found over most of the subtropical gyre in the North Atlantic (MNW), the heat input due to this Ekman pumping in the summer months can be as large or larger than the surface heat flux. This warming of the seasonal thermocline due to vertical advection in summer is evident in the upper ocean heat budget calculations in section 4.1 (Figures 4 and 6).

In deriving (7), MNW and MM95 assume that the thickness of the Ekman layer is much less than the depth of the seasonal thermocline, a reasonable assumption at midlatitudes. If the Ekman layer is much thinner than the seasonal pycnocline, then the heat gain over the total depth of the seasonal pycnocline will be approximately equal to the heat gain within the

seasonal pycnocline below the Ekman layer, resulting in (7). However, because the depth of the Ekman layer increases as f^{-1} and the depth of the seasonal pycnocline decreases as one approaches the southern limit of the subtropical gyre, it may not be a very good approximation at low latitudes. If the total heat gain in the seasonal pycnocline below the Ekman layer is assumed to be a fraction δ of the total heat gain from the surface to the base of the seasonal thermocline, then the modified heat flux through the base of the Ekman layer, H'_{net}, is related to the heat flux at the surface and the Ekman transports as

$$H'_{\text{net}} = \delta H_{in} + \delta \frac{C_w}{\alpha} \mathbf{U_E} \cdot \nabla \rho_m + (1 - \delta)w_E[\rho_s - \rho_m(t)]. \quad (9)$$

In the limit of a very thin Ekman layer, $\delta \to 1$, and (7) is recovered.

The total buoyancy flux available for subduction, equation (6), is now generalized to include the effects of (1) a finite thickness Ekman layer, (2) convergence of buoyancy due to subgrid-scale parameterizations, and (3) a diabatic main thermocline. The heat flux convergence within the seasonal thermocline due to parameterizations of mesoscale eddies is H_{eddy} and that due to the along-isopycnal subgridscale mixing is H_{iso}:

$$H_{\text{sub}} = \delta\left(\overline{H_{\text{net}}} - \overline{H_{\text{pump}}} + \overline{H_{\text{eddy}}} + \overline{H_{\text{iso}}} - \frac{C_w h_{ml}}{\alpha}\frac{D\rho_T}{Dt}\right). \quad (10)$$
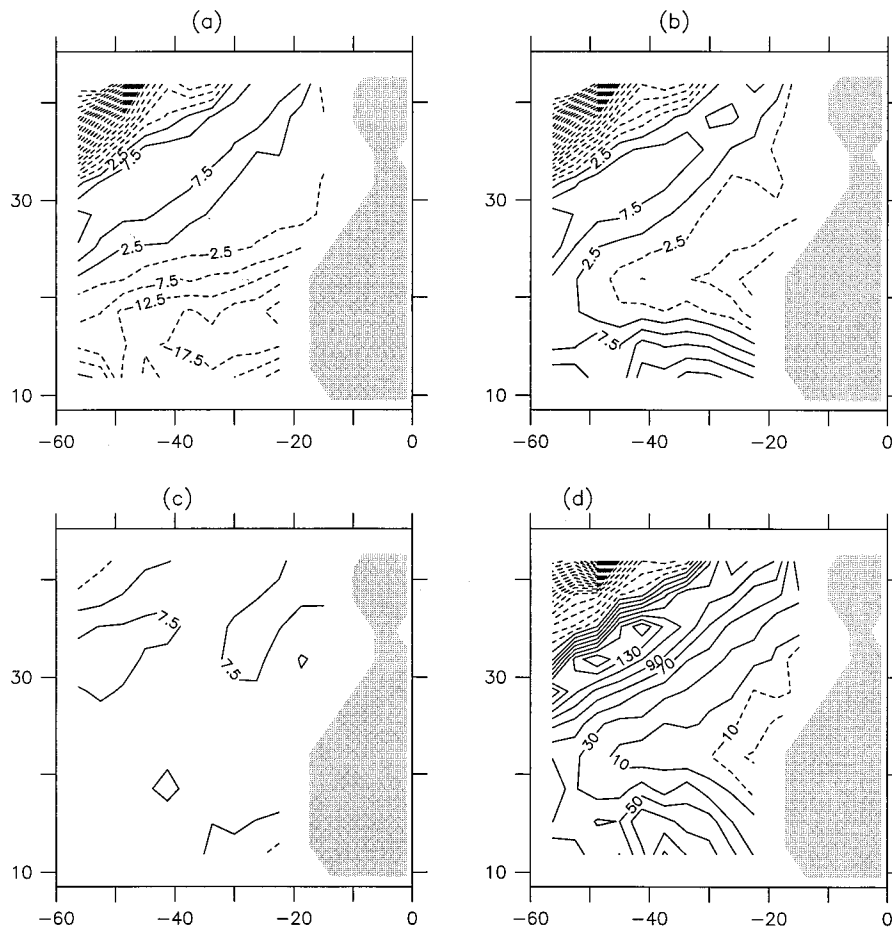
Figure 8. Terms contributing to the thermodynamic estimate of the annual subduction rate: (a) $\bar{H}_{in}$, (b) $\bar{H}_{net}$, (c) $-H_{pump}$ (W m^{-2}), and (d) approximate subduction rate (m yr^{-1}) based on (6) and (5).

The first two terms on the right-hand side are the same as were considered by MNW and MM95 (with $\delta = 1$). The additional terms represent the effects of eddy fluxes (H_{eddy}), along-isopycnal diffusion (H_{iso}), and the material derivative following the geostrophic flow in the main thermocline ($D\rho_T/Dt$). The effect of heat storage in the Ekman layer ($\delta < 1$) is to reduce the overall subduction rate.

The surface buoyancy flux $\bar{H}_{in}$, averaged over the 2 years of the calculation, is shown in Figure 8a. The surface heat flux in the model is positive and $O(10$ W m$^{-2})$ over most of the eastern subtropical gyre (Figure 1). However, in the eastern basin the evaporation exceeds the precipitation by about 1 m yr^{-1}, which is roughly equivalent to between 10 and 15 W m^{-2}. As a result, the buoyancy flux is negative over much of the eastern subtropical gyre.

The horizontal Ekman velocity transports warm water toward the north in the southern subtropical gyre and cold waters to the south in the northern subtropical gyre. This lateral buoyancy flux provides an additional source for warming the seasonal thermocline at low latitudes, which when added to the surface buoyancy flux, makes $\bar{H}_{net} > 0$ over much of the subtropical gyre (Figure 8b). As discussed above, the lateral Ekman transport warms the upper layer most strongly south of 20°N. MNW find a similar warming due to lateral Ekman transports at low latitudes.

The downward pumping of warm waters by the Ekman pumping velocity provides a buoyancy flux of $O(5-10$ W m$^{-2})$ with strongest values in the middle of the gyre, where the Ekman pumping is largest (Figure 8c). This contribution due to Ekman pumping is of the same order of magnitude as the surface heat flux, but it does not dominate the upper ocean heat budget. Although MNW find larger values of H_{pump}, this overall balance is consistent with the climatological analysis of MNW.

The annual mean subduction rate taking account only of the terms considered by MNW is estimated using $\bar{H}_{net}$ (Figure 8b), the Ekman pumping (Figure 8c), and (5) is shown in Figure 8d. We have also taken into account the net change in the MLD over the 2 year period due to temporary storage of buoyancy in the upper ocean. The storage term is small, however, with maximum values of $O(5-10$ m yr$^{-1})$ in the southern portion of the domain. Because the effective subduction period is so short, the MLD h is taken to be the maximum mixed layer depth h_{ml}, and Q is calculated at the time of maximum MLD.

The overall subduction pattern and amplitudes are similar to those calculated using the kinematic method in section 5.1 (compare Figures 7d and 8d). The northwest region shows strong entrainment into the mixed layer in the vicinity of the Gulf Stream. There is a band of subduction rates exceeding 100 m yr^{-1} to the south and east of the Gulf Stream. This large gradient is due primarily to the gradient in the MLD h_{ml} rather than to gradients in the surface fluxes or Ekman transports. Both methods show increased subduction to the south, with values exceeding 50 m yr^{-1}; however, the thermodynamic
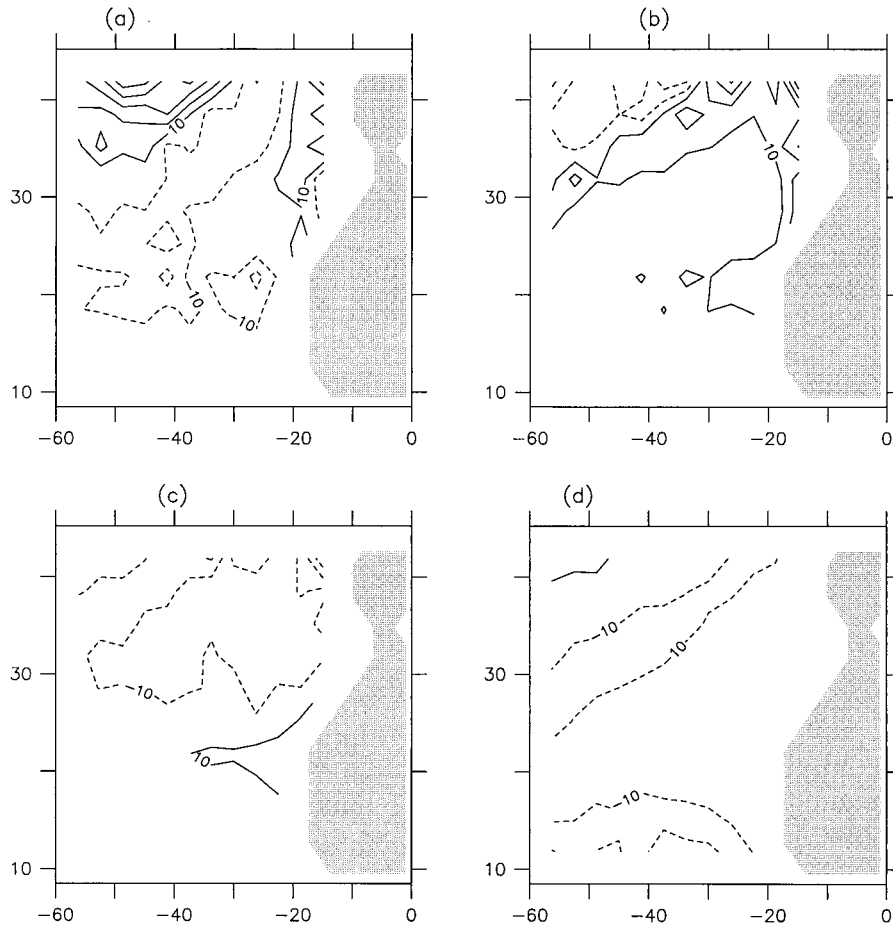
Figure 9. Contribution toward the annual subduction rate due to (a) diabatic thermocline, (b) the eddy buoyancy flux parameterization, (c) along-isopycnal diffusion, and (d) heat storage in the finite thickness Ekman layer (m yr^{-1}).

estimate increases to over 100 m yr^{-1} at 12°N. The subduction rate is negative in the far eastern basin at middle latitudes, similar to that found using the kinematic estimate; however, the region of negative subduction rates is weaker and located slightly farther north in the kinematic estimate. A similar region of negative subduction rates near the eastern boundary was found using the thermodynamic method and climatology by MNW.

The differences between the kinematic and thermodynamic estimates in the model can be largely reconciled by considering the influences of (1) a diabatic thermocline, (2) a finite Ekman layer thickness, and (3) the influences of subgridscale parameterizations. The effective change in the subduction rate resulting from density not being conserved within the permanent thermocline (because of vertical diffusion and subgridscale parameterizations) is shown in Figure 9a. The subduction rate is decreased by $O(10 \text{ m yr}^{-1})$ over the central subtropical gyre, largely because of the vertical diffusion of heat into the permanent thermocline (as discussed in section 4). This reduces the effective heat gain in the seasonal thermocline, as indicated by (4). The diabatic effects increase the subduction rate in the northwest region, near the Gulf Stream, primarily because of the subgridscale parameterization of mesoscale eddies restratifying the upper ocean.

The additional terms that influence the heat budget in the seasonal thermocline are shown in Figures 9b–9d. The contribution toward the total subduction rate resulting from the model subgridscale parameterizations is shown in Figures 9b and 9c. The impact of the eddy fluxes is generally small over most of the subtropical gyre, with values <10 m yr^{-1} (Figure 9b). The eddy fluxes are slightly larger near the Gulf Stream, with enhanced subduction rates to the south and reduced rates to the north. The diffusion of tracers along isopycnal surfaces decreases the subduction rate by $O(10 \text{ m yr}^{-1})$, except near the southern limit of the subtropical gyre, where the subduction rate is slightly increased.

The influence of a finite Ekman layer thickness is demonstrated by taking the ratio of the heat gain within the seasonal pycnocline below the Ekman layer to the total heat gain within the seasonal pycnocline to be proportional to the ratio of the Ekman layer thickness to the depth of the seasonal thermocline,

$$\delta = \frac{\int_{h_{ml}}^{h_{ek}} D\rho_m/Dt}{\int_{h_{ml}}^{0} D\rho_m/Dt} = 1 - h_{ek}/h_{ml}. \quad (11)$$

While it is difficult to calculate the thickness of the Ekman layer precisely in a model in which the vertical viscosity changes rapidly in depth and in time, a useful approximation is
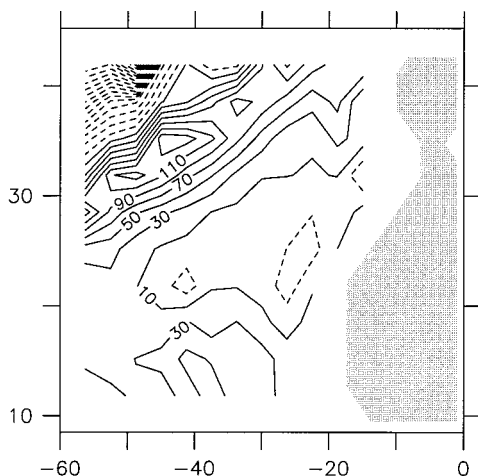
Figure 10. The total thermodynamic estimate of the subduction rate taking into account the effects of a diabatic thermocline, subgridscale parameterizations, and a finite Ekman layer thickness (Figures 9a–9d) (m yr^{-1}) on the basis of (10) and (5).

$h_{ek} = (2A_v/f)^{1/2}$, where $A_v = 66.7 \times 10^{-4}$ m^2 s^{-1} is the maximum vertical viscosity at the base of the mixed layer (due to internal wave breaking and shear instabilities). The thickness of the Ekman layer varies from 19 m at 12°N to 11.6 m at 41°N. The MLD shallows to $O(40$ m$)$ at 35°W, 12°N. The net effect of the finite Ekman layer thickness on the total subduction rate is shown in Figure 9d. The subduction rate is decreased by $O(5$ m yr$^{-1})$ over the interior of the subtropical gyre. The region of large subduction rates just southeast of the Gulf Stream, where the mixed layer shoals, are decreased by ~15 m yr^{-1}. The largest effect is found in the region of shallow mixed layers at low latitudes, where the total subduction rate is decreased by over 45 m yr^{-1}. This is the region where very large subduction rates were estimated using the original thermodynamic formulation and were also implied by the thermodynamic method of MNW but were not found using the more accurate kinematic method.

The thermodynamic estimate of the total subduction rate, calculated taking into account a finite Ekman layer thickness, subgridscale processes, and a diabatic thermocline, equation (10), is shown in Figure 10. The overall pattern is similar to the original estimate based on the idealized calculations of MNW; however, the modified estimate now agrees much more closely with the kinematic estimate from the model. The region of very large subduction rates found at low latitudes is greatly reduced, with the maximum now near 50 m yr^{-1}. The region of weak negative subduction has been decreased in amplitude near the eastern boundary and shifted slightly toward the north, in better agreement with the kinematic calculation. Finally, the region just to the south of the Gulf Stream has weaker subduction rates, also in better agreement with the kinematic result.

6. Summary and Conclusions

The upper ocean heat budget and subduction rates in the eastern North Atlantic have been diagnosed in a global, non–eddy-resolving general circulation model (the NCAR CSM ocean model). The purposes of this study are to explore the dynamics and thermodynamics that control the mean and seasonal to interannual variability of the thermal structure within the seasonal thermocline, to estimate the rates at which waters from the mixed layer are subducted into the permanent thermocline, and to evaluate how well a low-resolution general ocean circulation model can reproduce the observed upper ocean thermal structure over a 2 year period. The simulated mean and seasonal to interannual variability of SST and MLD compare well with mooring measurements at five locations within the subtropical gyre taken during the period of the Subduction Experiment (June 1991 through July 1993), although some problems in the model are suggested in the southeastern portion of the array.

The seasonal cycle is dominated by a one-dimensional balance between local surface fluxes and vertical mixing. However, advective processes are essential for maintaining the long-term mean thermal structure and for balancing the net heat exchange with the atmosphere throughout the subtropical gyre on a seasonal timescale. In the center of the gyre, vertical advection cools the surface and warms the seasonal thermocline, primarily through Ekman pumping in the summer. In the southern portion of the subtropical gyre, warming through lateral Ekman transport overcomes the cooling effect of Ekman pumping. This advective warming in the south and advective cooling in the central and northern gyre are balanced by vertical diffusion into the seasonal thermocline. A parameterization of the eddy heat flux due to baroclinic instability [*Gent and McWilliams*, 1990] weakly restratifies the seasonal thermocline with warming near the surface and cooling below. The net heat flux into the ocean is diffused vertically below the base of the seasonal thermocline, where it is balanced by advection of cold waters from the north.

The rate at which water is subducted from the mixed layer into the permanent thermocline has been estimated using both kinematic and thermodynamic methods. The overall pattern and rate of subduction are consistent with previous estimates, with maximum rates exceeding 100 m yr^{-1} in the northern subtropical gyre and smaller values of 10 m yr^{-1} to 50 m yr^{-1} in the central and southern portions of the gyre. These estimates compare reasonably well with the 20–40 m yr^{-1} inferred from tritium-^{3}He by *Jenkins* [1998]. The weak subduction rates in the eastern central subtropical gyre are at least in part due to anomalously weak Ekman convergence during the period of the Subduction Experiment.

As might be anticipated from their importance in the upper ocean heat budget, heat transport by lateral and vertical Ekman velocities are important components in the subduction process. A thermodynamic estimate of the subduction rate was derived that takes into account a finite thickness Ekman layer. It was found that neglecting this heat storage term results in an overestimate of the subduction rate at low latitudes (where the mixed layer shallows and the Ekman layer deepens) by ~100%. The influences of subgridscale parameterizations and a diabatic thermocline in the model are also calculated and found to be small but not negligible.

References

Cushman-Roisin, B., *Dynamics of the Oceanic Surface Mixed Layer*, edited by P. Muller and D. Henderson, *Hawaii Inst. of Geophys.*, Honolulu, 1987.

Danabasoglu, G., and J. C. McWilliams, Sensitivity of the global ocean circulation to parameterizations of mesoscale tracer transports, *J. Clim.*, 8, 2967–2987, 1995.

Gent, P. R., and J. C. McWilliams, Isopycnal mixing in ocean circulation models, *J. Phys. Oceanogr.*, 20, 150–155, 1990.

Gent, P. R., F. O. Bryan, G. Danabasoglu, S. C. Doney, W. R. Holland, W. G. Large, and J. C. McWilliams, The NCAR climate system model ocean component, *J. Clim.*, 11, 1287–1306, 1998.

Iselin, C. O., The influence of vertical and lateral turbulence on the characteristics of waters at mid-depth, *Eos Trans. AGU*, 20, 414–417, 1939.

Isemer, H.-J., and L. Hasse, *The Bunker Climate Atlas of the North Atlantic Ocean*, vol. 2, *Air-Sea Interactions*, 252 pp., Springer-Verlag, New York, 1987.

Jenkins, W. J., ^{3}H and ^{3}He in the beta triangle: Observations of gyre ventilation and oxygen utilization rates, *J. Phys. Oceanogr.*, 17, 763–783, 1987.

Jenkins, W. J., Studying subtropical thermocline ventilation and circulation using tritium and ^{3}He, *J. Geophys. Res.*, 103, 15,817–15,831, 1998.

Josey, S. A., A comparison of surface heat fluxes in the subduction region of the northeast Atlantic from the ECMWF and NCEP/NCAR reanalysis with moored buoy measurements, *J. Clim.*, in press, 2000.

Large, W. G., J. C. McWilliams, and S. C. Doney, Oceanic verical mixing: A review and a model with a nonlocal boundary layer parameterization, *Rev. Geophys.*, 32, 363–403, 1994.

Large, W. G., G. Danabasoglu, S. C. Doney, and J. C. McWilliams, Sensitivity to surface forcing and boundary layer mixing in the NCAR CSM ocean model: Annual-mean climatology, *J. Phys. Oceanogr.*, 27, 2418–2447, 1997.

Marshall, D., Subduction of water masses in an eddying ocean, *J. Mar. Res.*, 55, 201–222, 1997.

Marshall, D., and J. Marshall, On the thermodynamics of subduction, *J. Phys. Oceanogr.*, 25, 138–151, 1995.

Marshall, J. C., A. J. Nurser, and R. G. Williams, Inferring the subduction rate and period over the North Atlantic, *J. Phys. Oceanogr.*, 23, 1315–1329, 1993.

Montgomery, R. B., Circulation in upper layers of southern North Atlantic deduced with use of isentropic analysis, in *Papers in Physical Oceanography and Meteorology*, vol. VI(2), 55 pp., Mass. Inst. of Technol. and Woods Hole Oceanogr. Inst., Woods Hole, 1938.

Moyer, K. A., and R. A. Weller, Observations of surface forcing from the subduction experiment: A comparison with global model products and climatological datasets, *J. Clim.*, 10, 2725–2742, 1997.

Nurser, A. J., and J. C. Marshall, On the relationship between subduction rates and diabatic forcing of the mixed layer, *J. Phys. Oceanogr.*, 21, 1793–1802, 1991.

Rossow, W. B., and R. A. Schiffer, ISCCP cloud data products, *Bull. Am. Meteorol. Soc.*, 72, 2–20, 1991.

Spencer, R. W., Global oceanic precipitation from the MSU during 1979–91 and comparisons to other climatologies, *J. Clim.*, 6, 1301–1326, 1993.

Stommel, H., Determination of watermass properties of water pumped down from the Ekman layer to the geostrophic flow below, *Proc. Natl. Acad. Sci. U.S.A.*, 76, 3051–3055, 1979.

Williams, R. G., M. A. Spall, and J. C. Marshall, Does Stommel's mixed layer "demon" work?, *J. Phys. Oceanogr.*, 25, 3089–3102, 1995.

Woods, J. D., *Physics of Thermocline Ventilation: Coupled Atmosphere-Ocean Models*, edited by J. C. J. Nihoul, Elsevier Sci., New York, 1985.

P. W. Furey, M. A. Spall, and R. A. Weller, Department of Physical Oceanography, Woods Hole Oceanographic Institution, Mail Stop 21, Woods Hole, MA 02543. (spall@epl.whoi.edu)